VHCF response of heat-treated SLM Ti6Al4V Gaussian specimens with large loaded volume

Available online at www.sciencedirect.com

ScienceDirect

Procedia Structural Integrity 18 (2019) 314–321

Structural Integrity Procedia

www.elsevier.com/locate/procedia

25th International Conference on Fracture and Structural Integrity

VHCF response of heat-treated SLM Ti6Al4V Gaussian specimens with large loaded volume

A. Tridello[a]*, J. Fiocchi[b], C.A. Biffi[b], G. Chiandussi[a], M. Rossetto[a], A. Tuissi[b] and D.S. Paolino[a]

*[a] *Politecnico di Torino, Department of Mechanical and Aerospace Engineering, Corso Duca degli Abruzzi 24, 10129 Turin, Italy*
b National Research Council; Institute of Condensed Matter Chemistry and Technologies for Energy, Unit of Lecco, CNR ICMATE; Via G. Previati 1E, 23900 Lecco, Italy.

Abstract

Among the materials used for the production of components through Additive Manufacturing (AM) processes, the Selective-Laser-Melting (SLM) Ti6Al4V alloy is widely employed in aerospace applications for its high specific strength and in biomedical applications for its good biocompatibility. Actual structural applications are generally limited to static loading conditions where the large defects originating during the SLM process do not play a significant role for the static failure. On the contrary, the same defects strongly affect the fatigue response of the parts since they act as crack initiation sites that rapidly lead to fatigue failure. In the literature, a lot of research has been carried out to investigate the quasi-static and the High-Cycle Fatigue properties of the SLM Ti6Al4V alloy but there are still few studies on its Very-High-Cycle Fatigue (VHCF) response.
In the paper, the VHCF response of Ti6Al4V specimens, which are vertically orientated during the SLM building and then subjected to a conventional heat treatment (2 hours heating in vacuum at 850°C), is experimentally assessed. Ultrasonic VHCF tests are carried out on Gaussian specimens with a large risk-volume (2300 mm^3). Fracture surfaces are investigated for revealing the defect originating the fatigue failure. The Stress Intensity Factor Threshold associated to the experimental failures is finally estimated.

Peer-review under responsibility of the Gruppo Italiano Frattura (IGF) ExCo.

Keywords: Additive Manufacturing (AM); Selective Laser Melting (SLM); Very High Cycle Fatigue (VHCF); Ti6Al4V alloy.

* Corresponding author. Tel.: +39 011 0906913;
E-mail address: andrea.tridello@polito.it

2452-3216
Peer-review under responsibility of the Gruppo Italiano Frattura (IGF) ExCo.
10.1016/j.prostr.2019.08.171

1. Introduction

In the last few years, components produced through Additive Manufacturing (AM) processes are employed in an increasing number of applications, and, in many cases, are replacing components produced through traditional manufacturing processes. Steels, aluminum, titanium and NiCr alloys are currently used for the AM processes: among these AM materials, the AlSi10Mg and Ti6Al4V alloys are the most used and the most studied in the literature (Lewandowski and Seifi (2016)). In particular, Ti6Al4V is widely employed in aerospace applications for its high specific strength and in biomedical applications for its good biocompatibility. In order to be safely employed, the mechanical properties of AM Ti6Al4V parts must be properly assessed (Simonelli et al. (2014), Edwards and Ramulu (2014) and Fatemi et al. (2019)). Indeed, due to the manufacturing process, AM parts are characterized by a microstructure which is different from that of parts produced through traditional processes and, as a consequence, by different mechanical properties and strength. The development of safe and conservative design methodologies based on a proper experimental characterization is therefore a research subject of primary importance among universities and industries.

Quasi-static mechanical properties of Ti6Al4V parts produced through Selective Laser Melting (SLM) have been widely investigated in the literature (Shunmugavel et al. (2015) and Mower and Long (2016)). In particular, a proper optimization of the process parameters permits to manufacture SLM Ti6Al4V parts characterized by very good quasi-static mechanical properties that can outperform those assessed on parts manufactured with traditional non-additive technologies (Shunmugavel et al. (2015) and Mower and Long (2016)). On the contrary, High Cycle Fatigue (HCF) and Very High Cycle Fatigue (VHCF) loads are critical for AM parts, since the large defects originating during the SLM process represent an ideal crack initiation site, thus affecting the fatigue response. In the literature, there are still few studies on the VHCF response of the SLM Ti6Al4V alloy: in particular, in Wycisk et al. (2015) the effect of the stress ratio, of a stress relief heat treatment and of the Hot Isostatic Pressing (HIP) was analyzed, whereas in Günther et al. (2017) the VHCF response of hourglass specimens obtained through SLM and EBM was compared, with particular attention dedicated to the defects originated during the manufacturing process. In both papers, the experimental tests were carried out on hourglass or dog bone specimens machined to the final shape after the AM manufacturing process.

In the present paper, the VHCF response of SLM Ti6Al4V specimens, which are produced with a vertical growth orientation, is investigated. Ultrasonic VHCF tests are carried out on Gaussian specimens with a large loaded volume (2300 mm^3) and subjected to a conventional heat treatment performed in vacuum at 850°C for 2 hours after the building process. Differently from published literature results, Wycisk et al. (2015) and Günther et al. (2017), the specimens are not machined to obtain the final shape, but manually polished with the aim of not removing large defects concentrated near the surface and investigate the effect of all the defects on the VHCF response. Moreover, according to Fatemi et al. (2019), a large risk-volume is tested to take into account size-effect, which is shown to affect the VHCF response of Ti6Al4V alloy. Fracture surfaces are investigated with the Scanning Electron Microscope (SEM) and the defects originating the fatigue failure are analyzed. The crack propagation threshold of the tested specimens is finally investigated.

Nomenclature

VHCF	Very High Cycle Fatigue
SLM	Selective Laser Melting
V_{90}	risk-volume, region of material subjected to a stress amplitude above the 90% of the maximus stress
s_{local}	stress amplitude at specimen center
s_{local}	stress amplitude at the defect location (local stress amplitude)
N_f	Number of cycles to failure
FGA	Fine Granular Area
SIF	Stress Intensity Factor
K_d	SIF associated to the defect originating failure (or to the FGA)
K_{th}	SIF threshold

2. Materials and Methods

In the present Section the experimental activity is described: in Subsection 2.1 the powder chemical composition and the SLM process parameters are reported and the heat treatment and the quasi-static mechanical properties are described. In Subsection 2.2 the ultrasonic fatigue testing configuration is described.

2.1. Materials and SLM process parameters

Specimens for the tensile tests and the ultrasonic fatigue tests are produced by using a Renishaw AM400 system with standard process parameters and average powder size equal to 45 μm. Table 1 summarizes the process parameters adopted for the specimen production.

Table 1. SLM process parameters

Power	Exposure time	Layer thickness	Scanning strategy	Spot size	Point distance
400 W	60 μs	60 μm	Meander	65 μm	80 μm

After the manufacturing process, specimens are subjected to a traditional heat treatment, involving holding at 850 °C for 1 hour, followed by cooling in flowing Ar atmosphere. The resulting microstructure is characterized by a lamellar α + β mixture, deriving by the original acicular microstructure, which decomposed upon holding below the β transus temperature.

Quasi-static mechanical properties are also assessed by using a MTS 2/M machine with a 0.015 min^{-1} strain rate. The difference between the yield stress (849 MPa and 846 MPa) and the tensile strength (913 and 911 MPa) obtained in the two tests is limited and smaller than 5 MPa, whereas it increases slightly by considering the elongation to failure (4.7% in test 1 and 4.3% in test 2). These values are slightly smaller than the corresponding values obtained in the literature for Ti6Al4V specimens subjected to a similar heat treatment, Leuders et al. (2013): the limited difference (about 4.7%) could be due to the lower heating temperature (800° C) in Leuders et al. (2013) and, mainly, due to the different SLM process parameters considered for the specimen production.

The Vickers hardness is also measured and results to be 384.7 ± 4.1 HV.

2.2. Ultrasonic testing configuration

According to Pegues et al. (2018) and Fatemi et al. (2019), the specimen gage diameter and, accordingly, the risk volume, affect the High Cycle Fatigue response of AM Ti6AL4V specimens. Therefore, in order to take into account the size-effect, which is known to detrimentally affect the VHCF response of wrought parts, Furuya (2011), Tridello et al. (2015), Tridello et al. (2016) and Tridello et al. (2017), ultrasonic fatigue tests are carried out on Gaussian specimens, Paolino et al. (2014), Tridello et al. 2015, with a risk-volume V_{90} (according to the definition in Murakami (2002)) of 2034 mm^3. Differently from Wycisk, et al. (2015) and Fatemi et al. (2019), Gaussian specimens are not machined to the final shape, but are manually polished with sandpaper with increasing grit (from 240 to 1000). According to Tridello et al. (2018) and Tridello et al. (2019) and to the VHCF literature, the manual polishing process permits to avoid the crack nucleation due to the high surface roughness, whereas it does not eliminate dangerous surface defects and permits to investigate the role of both surface and internal defects on the VHCF response.

The geometry of the tested Gaussian specimens is shown in Fig. 1. The final roughness R_a, after the polishing process, is equal to 1.59 ± 0.19 μm.

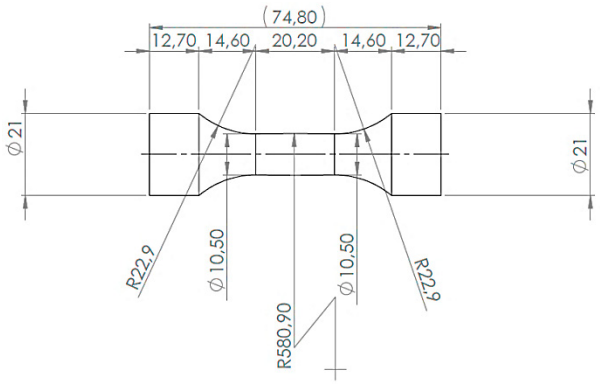

Fig. 1. Geometry of the Gaussian specimens used for the ultrasonic tests.

The ultrasonic testing machines developed at the Politecnico di Torino and available at the Dynlab of the Department of Mechanical and Aerospace Engineering are used for tests. Fully reversed tension-compression tests at constant stress amplitude are carried out up to failure or to 10^9 cycles (runout number of cycles). The displacement amplitude at the specimen free end, u_{end}, is continuously monitored during the experimental tests and is used as a feedback signal for keeping constant the stress amplitude at the specimen center. The correlation between u_{end} and the stress amplitude at the specimen center, s_{center}, is assessed through strain gage calibration. The temperature at the specimen center, monitored during the experimental test by using an infrared sensor, is kept below $25°$ C by using two vortex tubes. For further details on the ultrasonic fatigue testing equipment, the reader is reffered to Tridello (2017) and Tridello et al. (2017).

3. VHCF test results

In this Section, the experimental results are analyzed in details. In Subsection 3.1 the experimental dataset is reported. In Subsection 3.2 and 3.3, the fracture surfaces and the defects at the origin of the fatigue failure (location, type and size) are investigated, respectively. Finally, in Subsection 3.4 the Stress Intensity Factor (SIF) associated to the defects originating failure is investigated.

3.1. Experimental results

Sixteen ultrasonic fatigue tests are carried out: 10 specimens failed due to surface and internal defects, 4 specimens did not fail at 10^9 cycles (runout specimens) and 2 specimens failed at a number of cycles below 10^4 due to a large scratch which was not removed with the polishing process and, therefore, are not considered in the following analysis. In particular, by considering the valid data, 8 out of 10 failures originated from surface defects, whereas 2 out of 10 failures originated from an internal defect with the fracture surface showing a fish-eye morphology, Günther et al. (2017). Tests are carried out at increasing s_{center}, in the range [140 MPa - 220 MPa].

Fig. 4 shows the S-N plot of the experimental data: the local stress amplitude at the defect location, s_{local}, assessed through Finite Element Analysis (FEA), is reported in Fig. 2 in place of s_{center}, in order to take into account the actual stress involved in the crack nucleation process. Moreover, two markers are used for differentiating the fatigue failures originating from surface and internal defects.

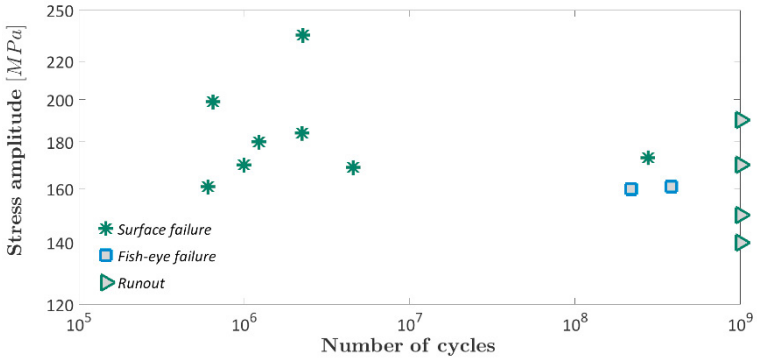

Fig. 2. S-N plot of the experimental data obtained by considering s_{local}.

According to Fig. 2, the scatter of the experimental failures is large and it is mainly related to the random distribution of the size of the defects originating failure. Tests are carried out at increasing levels of s_{center}, to investigate the fatigue response of the tested Ti6Al4V alloy at very large number of cycles: however, a clear monotonic decreasing trend cannot be seen in Fig. 2 and all the fatigue failures originated at s_{local} in the range 180 MPa $\pm$ 20 MPa (a part from 1 failure), with a very large scatter associated to the number of cycles to failure (failures between $6.4 \cdot 10^5$ and 10^9 cycles). On the other hand, Fig. 2 highlights that failures due to surface defects are characterized by a significantly smaller life (below 10^7 cycles), whereas internal defects originated a fatigue failure characterized by a longer life, in agreement with literature results Günther et al. (2017). The reason for the different fatigue life of surface and internal defects will be investigated in Section 3.4 by considering the Stress Intensity Factor.

3.2. Fracture surfaces

Fracture surfaces are investigated by using the optical microscope and the Scanning Electron Microscope (SEM). Fig. 3 shows the two types of fracture surfaces that are found experimentally: Fig. 3a shows a fatigue failure originating from a surface defect; Fig. 3b and Fig. 3c show an example of the fish-eye morphology and a magnification of the defect originating the fish-eye morphology, respectively.

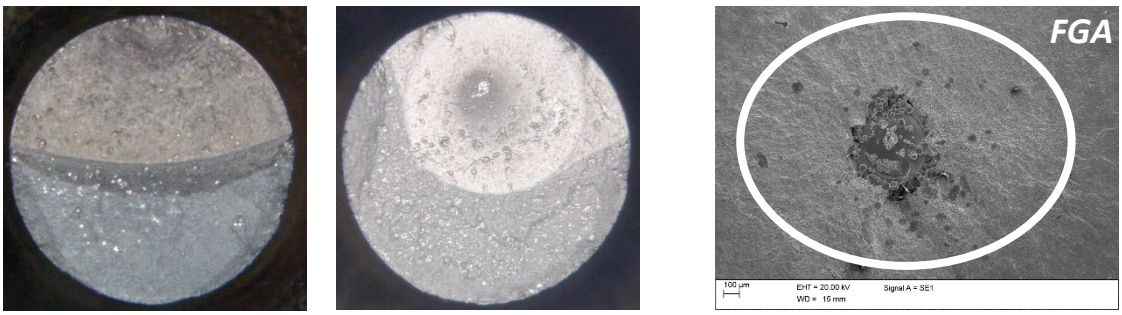

(a) (b) (c)

Fig. 3. Example of fracture surfaces found experimentally: (a) failure form surface defect; (b) fish-eye morphology; (c) magnification of the initial defect surrounded by the Fine Granular Area (FGA).

In Fig. 3a, the typical fracture surface of a fatigue failure originating from a surface defect can be observed: the crack originated from a defect close to the surface and then propagated inside the specimen. In Fig. 3b the crack started propagating from an internal defect due to incomplete fusion (Fig. 2c) and formed a fracture surface with a fish-eye morphology typical of VHCF failures and similar to those found in Günther et al. (2017). In Fig. 3c the initial defect and the surrounding Fine Granular Area (FGA) are shown: in particular, the crack originated from the defect up to the border of the FGA and then starts propagating according to traditional mechanisms.

3.3. Defect analysis

Fig. 4 shows an example of the defects originating the fatigue failures found experimentally. Fig. 4a shows a defect formed due to insufficient bonding between successive layers, whereas Fig. 4b shows a defect due to incomplete fusion, as suggested by the presence of numerous unmelted powder particles.

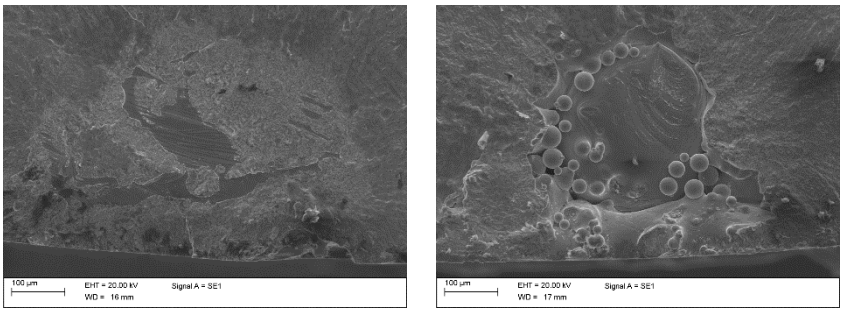

(a) (b)

Fig. 4. Types of defects at the origin of the fatigue failures: (a) defect due to insufficient bonding between successive layers; (b) defect due to incomplete fusion.

The defects originating the fatigue failures are similar to those found in the literature for Ti6Al4V alloy, Günther et al. (2017) and Masuo et al. (2018): in particular, almost all the fatigue failures (9 out of 10) originated from defects due to incomplete fusion and defects due to insufficient layer bonding, whereas only one fatigue crack originated from a group of superficial pores. The defect size $\sqrt{a_c}$, computed by considering the equivalent defect size according to Murakami (2002), is within the range $[379: 692]$ µm and is generally larger than that found in Günther et al. (2017). This could be due to the fact that in the present research the specimens are not machined and, therefore, large superficial defects are not removed. The different process parameters can also be the reason for the different defect size and morphology. Moreover, the larger size of the defects found in the present paper can also be due to the significantly larger tested V_{90} (about 10 times larger than the maximum V_{90} tested in the literature).

3.4. Mode of failure: analysis of the SIF

In order to investigate the relation between the number of cycles to failure, N_f, and the failure mode, the Stress Intensity Factor associated to the defects originating the fatigue failure, K_d, is analyzed. K_d is computed according to Murakami (2002): $K_d = C \cdot s_{local} \cdot \left(\pi\sqrt{a_c}\right)^{0.5}$, being C a constant coefficient equal to 0.65 for surface defects and to 0.5 for internal defects. Fig. 5 shows the K_d computed for all the experimental failures with respect to the number of cycles to failure. For internal failures, the SIF is computed by considering the FGA size and is equal to the SIF threshold (K_{th}), according to Murakami (2002). The dotted gray line represents the mean value of the K_{th} estimated by considering the fish-eye failures.

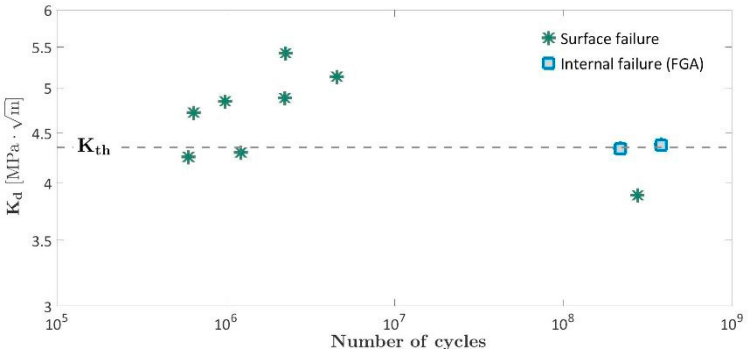

Fig. 5. SIF computed by considering the defect size (surface failure) and the FGA size (internal failure) with respect to number of cycles to failure

According to Fig. 5, 5 out of 10 surface failures originated from a defect with a K_d significantly larger than the K_{th}, thus justifying the N_f range below $2 \cdot 10^6$ cycles. 2 out of 8 surface failures are characterized by a defect with a SIF slightly smaller than the SIF threshold: however, due to the small amount of data, the scatter of the SIF threshold is not taken into account and it is probable that the SIF threshold for these two specimens is smaller than the average one estimated by considering the FGA. On the other hand, the surface failure which occurred at $2.7 \cdot 10^8$ cycles is characterized by a SIF significantly smaller than the estimated SIF threshold. A detailed analysis is in progress to highilight the possible presence of a local weaker region in the vicinity of the defect that originated the surface failure. This would justify a local decrement of the SIF threshold that permitted the crack growth for a small value of the defect SIF.

To conclude, experimental results confirm that, for the tested specimen condition (i.e., not machined and subjected to a manual polishing), surface defects control the VHCF response. In particular, if the surface defects are removed through a post-treatment process, the crack origin shifts to internal defects, with significantly larger fatigue life and a consequent enhancement of the VHCF response.

4. Conclusions

In the present paper, the VHCF response of Ti6Al4V specimens, produced through a SLM process and vertically oriented in the building platform was investigated. Ultrasonic VHCF tests were carried out on Gaussian specimens with large risk-volume ($2034\ \text{mm}^3$), subjected to a conventional heat treatment after the building process (heating in vacuum at 850°C for 2 hours) and thereafter to a manual polishing process in order to eliminate the effect of the high surface roughness and to investigate the effect of both surface and internal defects on the VHCF response.

Tests were carried out at increasing levels of stress amplitude, measured at the specimen center, in the range [140 MPa - 220 MPa] to investigate the VHCF response. The experimental data were analyzed by considering the local stress amplitude (stress amplitude at the defect location), in order to take into account the stress variation within the risk-volume. For the investigated range of stress amplitude, a clear monotonic decreasing trend between stress amplitude and number of cycles to failure was not found in the S-N plot, with failures concentrated in the range $180\ \text{MPa} \pm 20\ \text{MPa}$ (a part from 1 data) and a very large scatter associated to the number of cycles to failure (between $6.4 \cdot 10^5$ and 10^9). The reason for the large scatter associated to the VHCF resistance was found to be related mainly to the location of the initial defect. Indeed, surface defects originated fatigue failures with number of cycles to failure below $5 \cdot 10^6$; on the contrary, in 2 out of the 3 specimens that failed above $2 \cdot 10^8$ cycles, the fatigue crack originated from an internal defect, with the fracture surface showing a fish-eye morphology. The analysis with the Scanning Electron Microscope confirmed that the initial defects were the same for both internal and surface failures (bonding defects and defects due to incomplete fusion), thus highlighting the importance of eliminating surface defects. The Stress Intensity Factor associated to the defects was finally investigated and highlighted that the SIF

associated to surface defects was larger than the SIF threshold, thus justifying the fatigue failure range below $2 \cdot 10^6$ cycles for almost all the specimens showing a surface failure.

In conclusion, the experimental results confirmed that for the tested specimens, not machined and subjected to a manual polishing, surface defects control the VHCF response: if the surface defects are removed through a post-treatment process, the crack origin more likely shifts to internal defects, yielding a significantly larger fatigue life and a consequent enhancement of the VHCF response.

References

Edwards, P., Ramulu, M., 2014. Fatigue performance evaluation of selective laser melted Ti–6Al–4V. Materials Science and Engineering: A 598, 327-337. https://doi.org/10.1016/j.msea.2014.01.041

Fatemi, A., Molaei, R., Simsiriwong, J., Sanaei, N., Pegues, J., Torries, B., Phan, N., Shamsaei, N., 2019. Fatigue behaviour of additive manufactured materials: An overview of some recent experimental studies on Ti-6Al-4V considering various processing and loading direction effects. Fatigue & Fracture of Engineering Materials & Structures 42, 991-1009. https://doi.org/10.1111/ffe.13000

Furuya, Y., 2011. Notable size effects on very high cycle fatigue properties of high-strength steel. Materials Science and Engineering: A, 528 (15), 5234–5240. https://doi.org/10.1016/j.msea.2011.03.082

Günther, J., Krewerth, D., Lippmann, T., Leuders, S., Tröster, T. Weidner, A., Biermann, H., Niendorf, T., 2017. Fatigue life of additively manufactured Ti–6Al–4V in the very high cycle fatigue regime. International Journal of Fatigue 94 (Part 2), 236-245. https://doi.org/10.1016/j.ijfatigue.2016.05.018

Leuders, S., Thöne, M., Riemer, A., Niendorf, T., Tröster, T., Richard, H.A., Maier H.J., 2013. On the mechanical behaviour of titanium alloy TiAl6V4 manufactured by selective laser melting: Fatigue resistance and crack growth performance. International Journal of Fatigue 48, 300-307. https://doi.org/10.1016/j.ijfatigue.2012.11.011

Lewandowski, J.J., Seifi, M., 2016. Metal Additive Manufacturing: A Review of Mechanical Properties. Annual Review of Materials Research 46, 151-186. https://doi.org/10.1146/annurev-matsci-070115-032024

Masuo, H., Tanaka, Y., Morokoshi, S., Yagura, H., Uchida, T., Yamamoto, Y., Murakami, Y., 2018. Influence of defects, surface roughness and HIP on the fatigue strength of Ti-6Al-4Vmanufactured by additive manufacturing. International Journal of Fatigue 117, 163–79. https://doi.org/10.1016/j.ijfatigue.2018.07.020

Mower, T.M., Long, M.J., 2016. Mechanical behavior of additive manufactured, powder-bed laser-fused materials. Materials Science and Engineering: A 651, 198-213. https://doi.org/10.1016/j.msea.2015.10.068

Murakami, Y. (2002) Metal Fatigue: Effects Of Small Defects And Nonmetallic Inclusions. Elsevier Ltd, Oxford, UK.

Paolino, D. S., Tridello, A., Chiandussi, G., Rossetto, M., 2014. On specimen design for size effect evaluation in ultrasonic gigacycle fatigue testing Fatigue & Fracture of Engineering Materials & Structures 37 (5), 570-579. https://doi.org/10.1111/ffe.12149

Pegues, J., Roach, M., Williamson, R.S., Shamsaei N., 2018. Volume Effects on the Fatigue Behavior of Additively Manufactured Ti-6Al4V Parts. the 29th Annual Solid Frefform Fabrication Symposium Proceedings, Austin, TX.

Shunmugavel, M., Polishetty, A., Littlefair, G. 2015. Microstructure and mechanical properties of wrought and Additive manufactured Ti-6Al-4V cylindrical bars. Procedia Technology 20, 231-236. https://doi.org/10.1016/j.protcy.2015.07.037

Simonelli, M., Tse, Y.Y., Tuck, C., 2014. Effect of the build orientation on the mechanical properties and fracture modes of SLM Ti–6Al–4VM. Materials Science and Engineering: A 616, 1-11. https://doi.org/10.1016/j.msea.2014.07.086

Tridello, A., Paolino. D.S., Chiandussi, G., Rossetto, M., 2015. Gaussian Specimens for Gigacycle Fatigue Tests: Evaluation of Temperature Increment. Key Engineering Materials 625, 85–88. https://doi.org/10.4028/www.scientific.net/KEM.627.85

Tridello, A., Paolino. D.S., Chiandussi, G., Rossetto, M., 2015. VHCF Response of AISI H13 Steel: Assessment of Size Effects through Gaussian Specimens. Procedia Engineering 109, 121–127. https://doi.org/10.1016/j.proeng.2015.06.218

Tridello, A., Paolino, D.S., Chiandussi, G., Rossetto, M., 2016. VHCF strength decrement in large H13 steel specimens subjected to ESR process. Procedia Structural Integrity 2, 1117–1124. https://doi.org/10.1016/j.prostr.2016.06.143

Tridello, A., 2017 VHCF response of Gaussian specimens made of high-strength steels: comparison between unrefined and refined AISI H13, Fatigue & Fracture of Engineering Materials & Structures 40 (Issue 10), 1676–1689. https://doi.org/10.1111/ffe.12610

Tridello, A., Paolino, D.S., Chiandussi, G., Rossetto, M., 2017. Effect of electroslag remelting on the VHCF response of an AISI H13 steel. Fatigue & Fracture of Engineering Materials & Structures 40 (11), 1783–1794. https://doi.org/10.1111/ffe.12696

Tridello, A., Biffi, C.A., Fiocchi, J., Bassani, P., Chiandussi, G., Rossetto, M., Tuissi, A., Paolino, D.S., 2018. VHCF response of as-built SLM AlSi10Mg specimens with large loaded volume. Fatigue & Fracture of Engineering Materials & Structures; 41, 1918–1928. https://doi.org/10.1111/ffe.12830

Tridello, A., Fiocchi, J., Biffi, C.A., Chiandussi, G., Rossetto, M., Tuissi, A., Paolino, D.S., 2019. VHCF response of Gaussian SLM AlSi10Mg specimens: Effect of a stress relief heat treatment. International Journal of Fatigue 124, 435-443. https://doi.org/10.1016/j.ijfatigue.2019.02.020

Wycisk, E., Siddique, S., Herzog, D., Walther, F., Emmelmann, C., 2015. F.atigue Performance of Laser Additive Manufactured Ti–6Al–4V in Very High Cycle Fatigue Regime up to 10^9 Cycles. Frontiers in Materials 2 (72), 1-8. doi.org/10.3389/fmats.2015.00072.